Glutamate 107 in Subunit I of Cytochrome *bd* from *Escherichia coli* Is Part of a Transmembrane Intraprotein Pathway Conducting Protons from the Cytoplasm to the Heme b_{595}/Heme *d* Active Site[†]

Vitaliy B. Borisov,[‡,§] Ilya Belevich,[‡,||] Dmitry A. Bloch,[||] Tatsushi Mogi,[⊥] and Michael I. Verkhovsky*[,||]

Department of Molecular Energetics of Microorganisms, Belozersky Institute of Physico-Chemical Biology, Lomonosov Moscow State University, Moscow 119991, Russian Federation, Helsinki Bioenergetics Group, Institute of Biotechnology, University of Helsinki, PB 65 (Viikinkaari 1), 00014, Helsinki, Finland, and Department of Biomedical Chemistry, Graduate School of Medicine, University of Tokyo, Hongo, Bunkyo-ku, Tokyo 113-0033, Japan

Received March 14, 2008; Revised Manuscript Received June 3, 2008

ABSTRACT: Cytochrome *bd* is a terminal quinol:O_2 oxidoreductase of the respiratory chain of *Escherichia coli*. The enzyme generates protonmotive force without proton pumping and contains three hemes, b_{558}, b_{595}, and *d*. A highly conserved glutamic acid residue of transmembrane helix III in subunit I, E107, was suggested to be part of a transmembrane pathway delivering protons from the cytoplasm to the oxygen-reducing site. When E107 is replaced with leucine, the hemes are retained but the ubiquinol-1-oxidase activity is lost. We compared wild-type and E107L mutant enzymes during single turnover using absorption and electrometric techniques with a microsecond time resolution. Both wild-type and E107L mutant cytochromes *bd* in the fully reduced state bind O_2 rapidly, but the formation of the oxoferryl species in the mutant is dramatically retarded as compared to the wild type. Intraprotein electron redistribution induced by the photolysis of CO bound to ferrous heme *d* in the one-electron-reduced wild-type enzyme is coupled to the membrane potential generation, whereas the mutant cytochrome *bd* shows no such potential generation. The E107L mutation also causes decrease of midpoint redox potentials of hemes b_{595} and *d* by 25−30 mV and heme b_{558} by ∼70 mV. There are two protonatable groups redox-linked to hemes b_{595} and *d* in the active site, one of which has been recently identified as E445, whereas the second group remains unknown. Here we propose that E107 is either the second group or a key residue of a proposed proton delivery pathway leading from the cytoplasm toward this second group.

The aerobic respiratory chain of *Escherichia coli* terminates with the two quinol oxidases, cytochrome bo_3 and cytochrome *bd* (*1, 2*). Cytochrome bo_3 (encoded by *cyo*ABCDE operon) predominates when the cells are grown with high aeration, and cytochrome *bd* (encoded by *cyd*AB operon)[1] is predominant when the oxygen tension is low (*6–8*). Both oxidases are primary generators of $\Delta\mu_{H^+}$ [2] (transmembrane difference in the electrochemical H^+ potentials), because the electron transfer from a substrate quinol to molecular oxygen to form water is directly coupled to the transmembrane charge separation (*9–12*). Cytochrome bo_3 is a proton pump and belongs to a superfamily of heme−copper oxidases (*13*). Cytochrome *bd* does not pump protons and has no copper (*13–16*). The *bd* enzyme has a remarkably high affinity for oxygen (*17*) and relatively low sensitivity to cyanide during turnover (*18–20*).

Cytochrome *bd* is a heterodimer containing subunit I (CydA) and subunit II (CydB) (*13–16*). The 3D structure of cytochrome *bd* has not been resolved yet. Meanwhile, neither of these subunits reveals sequence homology to any of subunits of cytochrome bo_3 or other heme−copper oxidases (*21, 22*). Cytochrome *bd* contains three heme groups, b_{558}, b_{595}, and *d*, which are predicted to locate close to the periplasmic side of the membrane (*23, 24*). A low-spin hexacoordinated heme b_{558} has H186 and M393 of subunit I as the axial ligands. It is supposed to locate near a quinol-binding site and mediate electron transport from the quinol to hemes b_{595} and *d* (*25, 26*). A high-spin heme *d* is the place

[†] This work was supported by Biocentrum Helsinki, the Sigrid Jusélius Foundation, the Academy of Finland (to I.B., D.A.B., and M.I.V.), and the Russian Foundation for Basic Research, Grant 08-04-00093 (to V.B.B.).

* To whom correspondence should be addressed. Tel: +358-9-191 58005. Fax: +358-9-191 59920. E-mail: Michael.Verkhovsky@Helsinki.Fi.

[‡] These two authors made equal contributions to the work.

[§] Lomonosov Moscow State University.

[||] University of Helsinki.

[⊥] University of Tokyo.

[1] The *E. coli* genome reveals a further operon (*cyx*AB, previously called *app*BC or *cbd*AB) encoding a *bd*-type quinol oxidase (*3*) that may be expressed under conditions close to anaerobiosis (*4*). Although the *cyx*AB-encoded enzyme has been isolated and characterized (*5*), it remains to be poorly studied and its physiological role is not known.

[2] Abbreviations: $\Delta\mu_{H^+}$, transmembrane difference in the electrochemical H^+ potentials; $\Delta\Psi$, electrical membrane potential; FTIR, Fourier transform infrared; E_m, midpoint redox potential; **R**, fully reduced species; **MV**, "mixed-valence" (one-electron-reduced) species; **A**, ferrous oxy species; **P**, peroxy species; **F**, oxoferryl species; **O**, fully ferric species; τ, time constant, reciprocal of rate constant; TMPD, *N*,*N*,*N*′,*N*′-tetramethyl-1,4-phenylenediamine; NHE, normal hydrogen electrode.

10.1021/bi800435a CCC: $40.75
Published on Web 07/03/2008

where O_2 is bound and reduced to H_2O. Although its axial ligand has not been identified, a highly conserved E99 subunit I could be a candidate (*27*). A high-spin pentacoordinated heme b_{595} has H19 of subunit I as the axial ligand. Heme b_{595} facilitates electron transfer from heme b_{558} to heme *d* (*28, 29*). In addition, it is believed that heme b_{595} is adjacent to heme *d* and that both hemes are arranged as a diheme oxygen-reducing site (*11, 12, 30–38*).

The *bd*-type oxidases are widely distributed among prokaryotes and play an important role in bacterial physiology. Notably, cytochrome *bd* was reported to enable both pathogenic and commensal bacteria to colonize oxygen-poor environments (*39–42*), increase virulence and survival in host mammalian cells (*43, 44*), and enhance bacterial tolerance to nitrosative stress (*45–47*). These properties make cytochrome *bd* particularly attractive for its mechanism of oxygen reduction and the chemistry-linked energy conservation to be studied on the molecular level.

Cytochrome *bd* generates $\Delta\mu_{H^+}$ by means of "vectorial chemistry", when oxidation of ubi(mena)quinol releases protons to the periplasmic (*positive*) side of the membrane, while the protons required for oxygen reduction to water are taken up from the cytoplasmic (*negative*) side of the membrane. Single-turnover electrometric experiments showed that membrane potential generation is associated with electron transfer from heme b_{558} to the b_{595}/*d* diheme active site (*10–12*). However, since all three hemes are likely to be located at the same depth of the membrane close to the periplasmic side (*23, 24*), the electron transfer itself cannot be electrogenic (*10*). Instead, the vectorial proton movement from the cytoplasm toward the active site on the opposite (periplasmic) side of the membrane coupled to the redox reaction between the hemes *b* and *d* must occur (*10–12*). The latter means that there must be a proton-conducting channel connecting the cytoplasm to the b_{595}/*d* diheme active site (*10, 11*). On the basis of sequence analysis, it was suggested that the highly conserved E99 and E107 in α-helix III of subunit I are parts of such channel (*23*).

Site-directed mutagenesis in combination with time-resolved electrometry and absorption spectroscopy are powerful tools for studying the role of individual amino acid residues in proton-conducting pathways in terminal oxidases and other energy transducers such as a light-driven proton pump bacteriorhodopsin (*48, 49*). Very recently, the mutations in E99 and E107 in subunit I of the *E. coli* cytochrome *bd* have been analyzed (*27, 50*). It appeared that all mutations at E99 site and some at E107 site (e.g., E107A and E107D) resulted in the loss of the hemes b_{595} and *d* (*27, 50*); therefore, these mutants are useless for time-resolved experiments. At the same time, the two E107 mutants (E107L and E107Q) retain the hemes (>50% heme *d* content) (*27, 50*). The mutants have very little (5%, E107L) or no (<1%, E107Q) ubuquinol-1-oxidase activity but retain quite substantial ascorbate/TMPD-oxidase activity (20−30%), as compared to the wild-type enzyme (*27, 50*). E99 and E107 appear to be critical for the assembly and/or stability of the b_{595}/*d* diheme active site (*27, 50*). Fourier transform infrared (FTIR) redox difference spectroscopy of the E107Q mutant enzyme reported that E107 in the wild-type enzyme is protonated at pH 7.6 and perturbed upon reduction of the b_{595}/*d* diheme active site (*50*).

In this work, we studied the E107L mutant cytochrome *bd* from *E. coli* by means of electrometry and absorption spectroscopy with a microsecond time resolution to elucidate the role of E107 in translocation of protons within the protein molecule.

MATERIALS AND METHODS

Purification of Wild-Type and E107L Enzymes. The wild-type cytochrome *bd* and the E107L mutant oxidases were isolated from *E. coli* strains ST4683/pNG2 (Δ*cyo*::Cm^R Δ*cyd*::Km^R/ *cyd*$^+$ Tet^R) and ST4683/pMFO9/pNG2-E107L (Δ*cyo*::Cm^R Δ*cyd*::Km^R/ *cyo*$^+$ Amp^R/ *cyd*$^-$ Tet^R), respectively, as described previously (*27*).

Heme analysis. The heme *b* contents of both wild-type and E107L mutant enzymes were measured by the pyridine hemochromogen assay, using a value of $\Delta\varepsilon_{556.5-540}$ of 23.98 $mM^{-1}\cdot cm^{-1}$ (*51*). The heme *d* content was determined from the reduced-*minus*-"air-oxidized" difference absorption spectra using $\Delta\varepsilon_{628-607}$ of 10.8 $mM^{-1}\cdot cm^{-1}$ (*32*). The concentration of heme b_{558} was estimated using the value of $\Delta\varepsilon_{561-580}$ of 21.0 $mM^{-1}\cdot cm^{-1}$ for the (dithionite-reduced)-*minus*-"air-oxidized" difference spectra (*31*). Since the amounts of the ferrous heme *d* oxy complex and the ferryl-oxo heme *d* species in the "air-oxidized" enzyme are variable, the heme *d* content of the wild-type and mutant oxidases was also determined by using $\Delta\varepsilon_{628-670}$ of 25 $mM^{-1}\cdot cm^{-1}$ for the dithionite-reduced absolute absorption spectra (*11*). Since not all "as prepared" cytochrome *bd* is in the one-electron-reduced (mixed-valence, **MV**) state, for CO photolysis measurements, the concentration of the CO-bound enzyme was estimated based on CO binding extinction coefficient of $\Delta\varepsilon_{643-623} = 13.2$ $mM^{-1}\cdot cm^{-1}$ for the difference spectra of the **MV** cytochrome *bd* (CO-bound-*minus*-deoxygenated). This $\Delta\varepsilon$ value was initially derived from the CO-bound/dithionite-reduced-*minus*-dithionite-reduced difference spectra.

Time-Resolved Spectrophotometric Measurements. Time-resolved spectrophotometric measurements were accomplished using a home-built CCD-based instrument as described in ref *52*. A pulsed 150 W xenon arc lamp (Applied Photophysics, Leatherhead, Surrey, U.K.) was used as the probe light source. The setup enables to record entire absorption spectra of 433 nm width (within 200−900 nm range) every 1 μs.

Cytochrome *bd* in either the **MV** state or fully reduced (**R**) state was prepared in a gastight cuvette. Deoxygenated **MV** enzyme was obtained by equilibration with argon gas using the vacuum/gas line. To obtain the **R** enzyme, the deoxygenated **MV** enzyme was further reduced under anaerobic conditions with 2.5 mM sodium ascorbate and 5 μM TMPD. To generate the CO-liganded enzyme, cytochrome *bd* in either the **MV** or **R** state was equilibrated with 1% CO/99% argon mixture. To perform the flow-flash experiments with the **R**−CO enzyme, the sample was transferred to the stopped-flow module (SFM-300, Bio-Logic, Claix, France) and then mixed with O_2-enriched water. CO photolysis was initiated by a laser flash (frequency-doubled YAG, 532 nm; pulse energy, 120 mJ; Brilliant B; Quantel, Les Ulis, France).

Time-Resolved Electrometric Measurements. Reconstitution of the wild-type and the E107L mutant enzymes into liposomes, preparation of the anaerobic samples, and direct

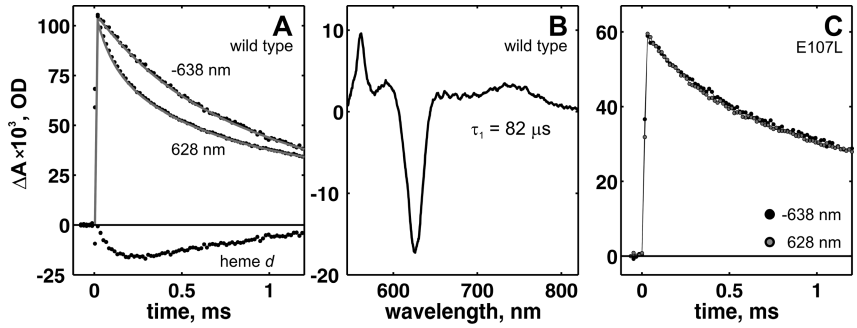

FIGURE 1: Optical changes following CO photolysis from the mixed-valence wild-type and E107L mutant cytochrome *bd*. (A) Wild-type kinetics of optical changes at 628 and 638 nm and their difference (heme *d*). The trace at 638 nm is an upside-down representation of the original data normalized to the trace at 628 nm by the amplitude of the CO photolysis phase. (B) Wild-type kinetic absorbance spectrum of the 82 μs phase. (C) E107L mutant kinetics of optical changes at 628 and 638 nm, presented similarly to that in panel A. The zero time is the moment of the laser flash. Conditions: CO-bound cytochrome *bd*, 15 μM (wild type), 12 μM (E107L mutant); Tween-20, 0.1%; HEPES−KOH (pH 7.5), 100 mM; CO, 1%.

electrical measurements with a microsecond time resolution were carried out essentially as reported (refs *10 –12 and references therein).*

The effective amount of **MV**−CO was ~45% for both the spectrophotometric and the electric measurements because not all "as prepared" cytochrome *bd* is in the **MV** state.

Spectroelectrochemistry. The spectropotentiometric redox titrations of both wild-type and the E107L mutant *bd*-type oxidases were performed by using an optically transparent, thin-layer electrode (OTTLE) cell as described (ref *53* and references therein). Potentials within the range of −100 to +450 mV *versus* NHE were set with ±20 mV steps during both oxidative and reductive titration using a PAR263A potentiostat (Princeton Applied Research, Oak Ridge, TN). At each potential step, the onset of equilibrium on the working electrode was determined. Two layers of gold minigrid (300 lpi, each layer with a 70% transmittance; Buckbee-Mears Europe GmbH, Germany) served as the working electrode. A platinum wire immersed in 3 M KCl and a saturated Ag/AgCl half-cell served as the counter electrode and reference electrode, respectively. Hexaammineruthenium (E_m = +50 mV), pentaaminepyridineruthenium (E_m = +250 mV), and ferrocenylethanol (E_m = +430 mV), all at 200 μM, were added as redox mediators. All redox potentials quoted refer to NHE.

Experimental Software and Data Analysis. Instrumental software for experimental setups was developed by N. Belevich (Helsinki, Finland). All measurements were performed at +21 °C. MATLAB (The Mathworks, South Natick, MA) was used for data analysis.

RESULTS

Electron Transfer Reactions with One-Electron-Reduced E107L Mutant and Wild-Type Enzymes. The basic understanding of the coupling between the electron and proton transfers may be obtained with the oxidase in the mixed-valence (one-electron-reduced) state. Under anaerobic conditions, a molecule of CO binds to heme *d* in the *bd* oxidase in the mixed-valence state and then can be easily dissociated by a flash of light. The photolysis of CO from heme *d* lowers the redox potential of this heme and, as a result, creates conditions for electron redistribution to other redox centers. This phenomenon is a very convenient as a tool for investigation of electron transfer reactions, and we used such approach to analyze the effect of E107L mutation on electron transfer in the *bd* oxidase from *E. coli*. The information gained from the studies of the oxidase in the mixed-valence state may facilitate deciphering the mechanism of the normal catalytic reaction. For this purpose, we applied a combination of two detection techniques: absorption spectroscopy and potentiometric electrometry.

The recording of the spectra every microsecond after the laser flash gives surface of absorbance data which can be decomposed into the kinetic components and spectra of the individual reactions. Figure 1A shows the selected traces of optical changes obtained from the surface of absorbance data during flash photolysis of CO from the mixed-valence wild-type enzyme. The trace at 628 nm (maximum of the ferrous heme *d* absorption spectrum) consists of the components reflecting two processes: oxidoreduction of heme *d* together with CO photolysis/recombination), while the second trace at 638 nm (note that the optical trace at 638 nm is an upside-down representation of the original data normalized to the trace at 628 nm by the amplitude of CO photolysis) is due to CO photolysis/recombination only. First, an initial sharp increase seen in both traces is due to kinetically unresolved phase of CO photolysis from heme *d*. At 638 nm, the CO dissociation phase is followed by two phases of CO recombination. Another trace, at 628 nm, is also dominated by CO recombination; however, at the same time an additional component, best seen as a difference between 628 and 638 nm curves, can be derived. This component represents oxidation and subsequent rereduction of heme *d* (Figure 1A, heme *d* trace).

From the fit of the complete surface of optical changes we were able to resolve the spectra of individual transitions and to establish their time constants. The three-exponential global fit with the time constants of about 80 μs, 375 μs, and 1.67 ms produced the best results. The spectrum of the 80 μs phase is shown in Figure 1B. It can be assigned to the pure electron backflow from heme *d* mostly to heme b_{595} (~80% of the electron goes to heme b_{595} and only ~20% to heme b_{558}), which is in agreement with a recent report (*11*). The amplitude of the electron backflow is relatively small (only about 11% of heme *d* gets oxidized by the *b*-hemes) but still detectable. The two slower phases (375 μs and 1.67 ms) are dominated by CO recombination. However, when the pure CO-recombination spectrum, obtained during CO photolysis of the fully reduced CO-bound cytochrome *bd*,

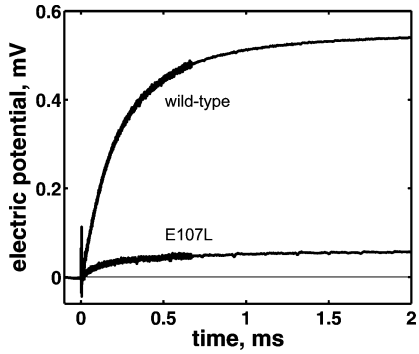

FIGURE 2: Electric potential generation upon CO photolysis from the mixed-valence wild-type (upper trace) and E107L mutant (lower trace) enzymes. The zero time is the moment of the laser flash. Conditions: MOPS−KOH (pH 7.0), 100 mM; glucose, 50 mM; catalase, 0.5 mg/mL; glucose oxidase, 1.5 mg/mL; CO, <1%.

is subtracted from the spectra of the slower phases, it reveals that heme *d* gets rereduced in the same time window. The spectra obtained after subtraction of CO-recombination spectrum from the slower phases (not shown) are essentially the same as the reversed spectrum shown in Figure 1B.

In contrast, no distinct electron backflow phase after CO photolysis from the mixed-valence state of the E107L mutant enzyme was observed. The flash photolysis of the mutant consists of only the two phases of CO recombination (Figure 1C). The CO dissociation is reverted with the two (rather than one) phases probably due to the low concentration of CO. At 1% CO in the gas phase, there is only 10 μM CO in the solution. In our experiments, the enzyme concentration was even higher than that of CO. To follow pseudo-first-order reaction (monoexponential decay), the concentration of CO should be much higher than the enzyme concentration. In our case, it was rather a bimolecular reaction that can be reasonably well fitted with two exponential components.

Electron Backflow Experiment with the One-Electron-Reduced E107L Mutant Enzyme Does Not Show $\Delta\Psi$ *Generation.* With electrometry it is possible to follow charge (electrons or/and protons) transfer that takes place perpendicular to the membrane plane. Thus electrometry supplements optical spectroscopy and may give information about proton translocation during the reaction. Figure 2 compares time courses of membrane potential generation after the flash-induced photolysis of CO from the mixed-valence wild-type (upper trace) and E107L mutant (lower trace) enzymes under anaerobic conditions. The electrometric response of the wild-type enzyme is very similar to that seen in a previous study (see Figure 5 in ref *10*). This $\Delta\Psi$ generation is coupled to the electron backflow from heme *d* to either or both hemes *b* (*10, 11*). In contrast, the mutant enzyme shows almost no $\Delta\Psi$ generation under the same experimental conditions (<10% of the total $\Delta\Psi$ amplitude of the wild-type enzyme). It is worthy to note that there is a relatively high difference in the rates of electric potential relaxation and CO recombination measured in the optical experiment. A possible explanation may be in the difference of the CO concentrations in the optical and electrometric experiments. While in the optical sample the concentration of CO is well defined and equilibrates rapidly with 1% of CO in the gas phase, in the electrometric cell the equilibration process is much slower due to design of the anaerobic box. Even though the gas phase in the electrometric box is the same (1% CO), it takes some time before CO reaches the sample. And during the measurements we see acceleration of electric potential dissipation due to CO recombination. Since the development of electric potential due to electron backflow is better seen in the slow relaxing sample, here we show the trace under such conditions.

Oxoferryl Species Is Not Observed in the Reaction of the Fully Reduced E107L Mutant Enzyme with O_2 *on the 100* μ*s Time Scale.* Figure 3 shows the kinetic difference spectra for the reaction of the wild-type and E107L mutant cytochromes *bd* in the fully reduced state with oxygen during the first 100 μs of the reaction. Both time constants and kinetic spectra for the wild-type enzyme are virtually identical to those observed in a recent study (*12*). The optical changes for the wild-type enzyme (Figure 3, left panel) correspond to three sequential transitions with τ of 1.4, 4.1, and 47 μs. The spectrum of the 1.4 μs phase reveals a minimum at 629−630 nm and a maximum at 653−654 nm that reflects the **R** → **A** transition. The spectrum of the 4.1 μs phase shows a trough at 653 nm and a peak at 634−635 nm that is due to the **A** → **P** transition (*12*). The spectrum of the 47 μs phase reveals minima at 560−562 and 639−640 nm and a maximum at 680 nm that is characteristic of the **P** → **F** transition.

For the E107L mutant enzyme, the development of the optical changes within the 100 μs time window can also be fitted by three-exponential transitions with time constants of 1.8, 7.5, and 56 μs (Figure 3, right panel). The spectrum of the 1.8 μs phase is identical to that of the first phase of the wild-type enzyme and therefore can be assigned to the **R** → **A** transition. The spectra of the 7.5 and 56 μs phases are essentially similar in line shape, but the amplitudes are small. Qualitatively, these spectra have features similar to the spectrum of the 4.1 μs phase of the wild-type enzyme (minima at about 560, 595, and 654 nm and a maximum around 635 nm). Hence we can conclude that these two spectra mainly reflect the **A** → **P** transition. It is most likely that, by the end of the 100 μs time window, the major part of the E107L enzyme is still in the **A** state. In the spectrum of the 56 μs phase, there is also a small maximum around 680 nm, and a peak at 635 nm is less pronounced as compared to the spectrum of the 7.5 μs phase (Figure 3, right panel). A tiny peak at 680 nm may point to a small contribution of the oxoferryl species formation to the spectrum of the 56 μs phase of the mutant enzyme that is consistent with a small counterpart electrogenic phase with τ of 85 μs (see below).

Single-Turnover Generation of $\Delta\Psi$ *by the Fully Reduced E107L Mutant Enzyme in the Reaction with* O_2 *Is Significantly Retarded As Compared to the Wild-Type Cytochrome bd.* We compared time courses of single-turnover $\Delta\Psi$ generation by the fully reduced wild-type and E107L mutant cytochromes *bd* from *E. coli* produced by their reactions with oxygen (Figure 4). In agreement with the previous work (*10–12*), the electrometric kinetics of the wild-type enzyme consists of the two parts, which are the faster nonelectrogenic (a "lag" phase; see Figure 4, Inset) and the slower, electrogenic. The lag phase comprises the two sequential electrically silent processes, the oxy complex formation (**R** → **A**), which is then followed by the peroxy complex formation (**A** → **P**) (*12*). The next **P** → **F** transition (conversion of peroxy intermediate to oxoferryl species) occurring with τ of 115

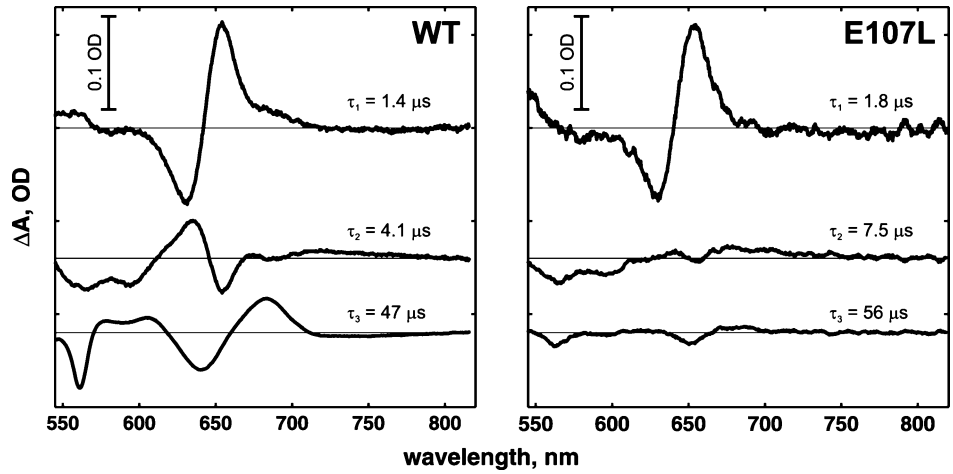

FIGURE 3: Reaction of the fully reduced wild-type (left panel) and E107L mutant (right panel) cytochromes *bd* with oxygen. Absorption spectra after flash-induced dissociation of CO from the enzyme in the presence of O_2 were recorded with 1 μs time resolution. Shown are the kinetic difference spectra of the corresponding reaction phases. Conditions: enzyme, 8.7 μM (wild type) or 8.3 μM (E107L mutant); O_2, 365 μM; CO, 5 μM; MOPS−KOH (pH 7.0), 100 mM; sodium ascorbate, 1.25 mM; TMPD, 2.5 μM; sucrose monolaurate, 0.1%. Concentrations quoted are for after 1:1 mixing. Optical path, 1 cm. For other conditions, see Materials and Methods.

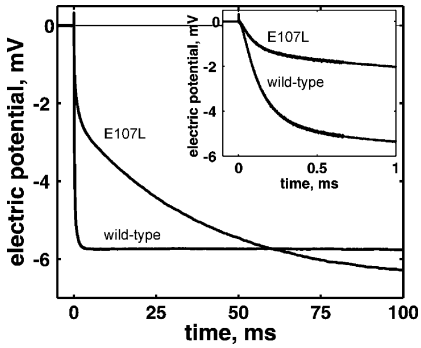

FIGURE 4: Electric potential generation by the fully reduced wild-type and E107L mutant cytochromes *bd* in reaction with O_2. Inset: Same transients shown in a shorter time scale. Conditions: MOPS−KOH (pH 7.0), 100 mM; TMPD, 10 μM; hexaammineruthenium, 10 μM; glucose, 50 mM; catalase, 0.5 mg/mL; glucose oxidase, 1.5 mg/mL; CO, 10 μM. Reaction was started by a laser flash after 450 ms from the beginning of injection of 100 μL of oxygen-saturated buffer ([O_2] = 1.2 mM).

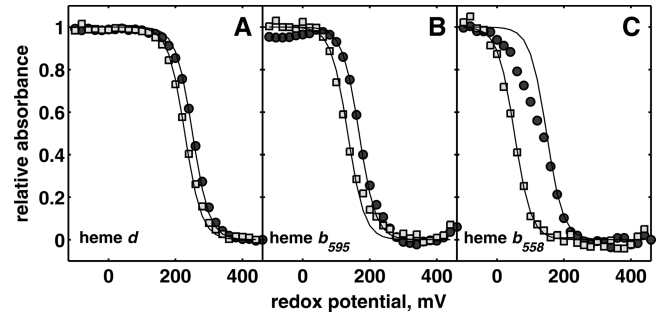

FIGURE 5: Spectroelectrochemical redox titrations of the wild-type (circles) and E107L mutant (squares) cytochromes *bd*. The titration profiles for hemes *d*, b_{595}, and b_{558} are shown at the wavelengths where the spectral contribution of each heme has a maximum (630, 575, and 530 nm, respectively). Each data point is the average of the oxidative and reductive titrations at matching potentials. Solid lines are one-electron Nernstian curves. The data points of the E107L cytochrome *bd* mutant (143 μM) are normalized to those of the wild-type cytochrome *bd* (156 μM). The measurements were performed in 0.084% sucrose monolaurate and 200 mM potassium phosphate buffer, pH 7.0. For other conditions, see Materials and Methods.

μs makes the major contribution to the electrogenic part (~75% of the total amplitude). The last phase of $\Delta\Psi$ generation (τ = 0.75 ms) is most likely due to the slowest transition (**F** → **O**) which takes place in a fraction of the enzyme that contains bound quinol (*11, 12*).

The electrometric response of the E107L mutant enzyme is clearly different from that of the wild-type enzyme (Figure 4). It also includes the initial nonelectrogenic and electrogenic parts but the $\Delta\Psi$ development is significantly retarded. As for the wild-type enzyme, the lag of the mutant cytochrome *bd* is due to the **R** → **A** and **A** → **P** transitions. The electrogenic part can be modeled by three exponentials with time constants of 85, 1.25, and 40 ms and relative amplitudes of about 20%, 20%, and 60%, respectively. These phases are possibly due to the **P** → **F** transition in different subpopulations of the E107L mutant enzyme.

E107L Mutation Decreases Redox Potentials of All Three Hemes, Especially Heme b_{558}. The spectroelectrochemical experiments consisted of the both reductive and oxidative titrations. At each fixed redox potential value in a range from −100 to +460 mV, the complete spectrum from 350 to 800 nm was collected, and as a result of a redox titration, we obtained wavelength-potential-absorbance surface. The titration data at characteristic wavelengths for the different hemes (*d*, b_{595}, and b_{558}) in the wild-type and E107L mutant cytochromes *bd* from *E. coli* are shown in Figure 5. The experimental points can be reasonably described with the Nernst n = 1 curves. In agreement with the previous reports (*54, 55*), the redox titration of heme b_{558} in the wild-type enzyme shows an additional low-potential fraction (Figure 5C). The results of redox titrations are summarized in Table 1. The E_m values of the hemes in the wild-type enzyme determined in this study are consistent with those reported earlier (ref *53* and references therein). The E107L mutation results in decrease of the E_m values of hemes b_{595} and *d* by 25−30 mV and heme b_{558} by ~70 mV.

DISCUSSION

We performed a comparative single-turnover study of the wild-type and E107L mutant cytochromes *bd* from *E. coli* using electrometry and absorption spectroscopy with a microsecond time resolution. The goal of this study was to

Table 1: Apparent Redox Midpoint Potentials of the Heme Groups of the Wild-Type and E107L Mutant *E. coli* Cytochromes *bd* Solubilized in 0.084% Sucrose Monolaurate

	E_m, mV (vs NHE)[a]	
heme	wild type	E107L mutant
b_{558}	+131	+58
b_{595}	+166	+136
d	+264	+239

[a] The standard deviation for the E_m values reported was ±5 mV.

elucidate the role of a highly conserved E107 of subunit I in translocation of protons through the membrane. We found that the mutant enzyme behaves differently from the wild-type enzyme in both the reaction of the fully reduced species with oxygen and the electron backflow with the **MV** species.

The reaction of the wild-type cytochrome *bd* in the **R** state with oxygen produces a membrane potential, which is negative inside the cell or proteoliposome. The main electrogenic event (with τ of 115 μs, Figure 4) occurs in the course of the **P** → **F** transition (Figure 3, left panel), in agreement with an earlier study (*12*). In contrast, almost no $\Delta\Psi$ generation in this time window is observed with the mutant enzyme under the same conditions (Figure 4). The major phase of $\Delta\Psi$ generation by the mutant cytochrome *bd* in the reaction with O_2 has a time constant of 40 ms, i.e., about 350 times slower than that of the wild-type enzyme. This is consistent with the fact that ubuquinol-1-oxidase activity of the E107L mutant is very low (~5% of the wild-type enzyme) (*27*). By the time when the reaction of the wild-type enzyme with oxygen yields oxoferryl species, the mutant cytochrome *bd* is still on the level of the **P** or even **A** species (Figures 3 and 4).

Photolysis of CO from the wild-type cytochrome *bd* in the **MV** state under anaerobic conditions results in the transient generation of $\Delta\Psi$, which is positive inside the cell or proteoliposome. Previously (*10*), we already conducted the study of the electron transfer reaction in the **MV** state of the *bd* oxidase but only at several specific wavelengths. However, the spectra of the hemes b_{558} and b_{595} are significantly overlapping (*54, 56*), and it is difficult to determine the extent and exact destination of the electron transfer. The application of the simultaneous kinetic recording in the whole visible range gave us a possibility to resolve this problem. The obtained surface of optical changes was the subject for global exponential fit to produce the kinetic spectra of individual events. The fit reveals a component with τ of about 80 μs that shows oxidation of ~11% of heme *d*. During this phase the electron simultaneously moves from heme *d* to hemes b_{595} and b_{558} in the proportion of 80%/20%, respectively. The same rate of electron transfer to both *b*-type hemes from the reduced heme *d* suggests that these two reactions have a common rate-limiting step. It is most likely the deprotonation of the group which is coupled to the oxidation of heme *d*. The predicted membrane topology for cytochrome *bd* (*23*) suggests that all three hemes are located at about the same depth in the membrane and electron transfer between them is unlikely to be electrogenic. At the same time, potential generation during the electron backflow reaction (ref *10* and this work) is very large when recounted on 100% of the oxidation of heme *d* and can account for a transfer of about complete charge through the membrane (*10*). Therefore, as enlightened by the electrometric results,

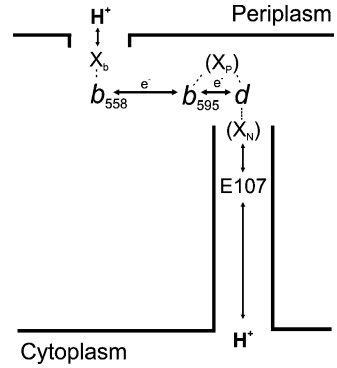

FIGURE 6: Schematic model of electron and proton transfer pathways in cytochrome *bd* from *E. coli*. There are two protonatable groups, X_P and X_N, redox-coupled to the heme b_{595}/heme *d* active site. A highly conserved E107 is a part of the channel mediating proton transfer to X_N from the cytoplasmic side of the membrane.

in particular by the H_2O/D_2O solvent isotope effect (*10*), the electron transfer from heme *d* to hemes *b* is coupled to proton release to the cytoplasmic side and proton uptake from the periplasmic side. The replacement of E107 abolishes the electron backflow reaction (Figure 2) and indicates the blockage of the proton release which is coupled to the oxidation of heme *d*.

Based on the amount of the CO-bound enzyme, the fraction of photolyzed heme *d* that was oxidized during electron equilibration is estimated to be ~11%. It is about twice smaller than the value (~25%) that we published earlier (*11*). Such difference could be explained by the fact that for the protein purification in ref (*11*) and in the current work (details of the purification can be found in ref *27*) the different protocols have been used.

There is no doubt that E107 is important for assembly and/or stability of the heme b_{595}/*d* binuclear site since the point mutation leads to complete (E107A, E107D) or partial (E107L, E107Q) loss of one or both redox components of the O_2-reducing site (*27, 50*). The question arises, whether this is the only role of E107? This work provides evidence that E107 is necessary for efficient catalysis of the reaction of oxygen reduction and membrane potential generation. The fact that $\Delta\Psi$ generation is significantly retarded in the forward oxygen reaction and nearly absent in the electron backflow experiment with the **MV** enzyme indicates that a proton donor−acceptor carboxylic group of the E107 residue can be involved in these processes. Based on the results of the present work, two possibilities may be suggested.

(1) E107 may be redox-coupled to heme b_{558}. For example, it may be part of a short proton channel connecting heme b_{558} to the periplasm (site X_b in Figure 6). Formation of heme *d*-oxoferryl species requires donation of an electron from heme b_{558} (*12*). Oxidation of heme b_{558} should be compensated by release of H^+ from a b_{558}-linked redox group to the periplasm via a putative short channel (*11*). If E107 was a part of such a channel, its replacement would lead to the impediment of b_{558} oxidation, and hence the **P** → **F** transition would be significantly inhibited. Similarly, electron backflow from heme *d* to heme b_{558} would be accompanied with proton uptake from the periplasm toward b_{558} that would be blocked by the mutation in E107. The fact that the E107L mutation dramatically decreases the E_m of heme b_{558} is in line with this hypothesis. It is known that electrons donated from

quinol are transferred to heme b_{558} and then to the b_{595}/d diheme site, whereas electrons donated from TMPD are transferred directly to the b_{595}/d site bypassing the quinol-binding site and heme b_{558} (*57*). Therefore, the finding that E107 mutant cytochromes *bd* with heme contents similar to the wild-type enzyme (E107L, E107Q) reveal virtually no ubiquinol oxidase activity but retain substantial TMPD-oxidase activity (up to one-third as compared to the wild-type enzyme) (*27, 50*) is also consistent with the above proposal. However, our data on electron backflow show that the E107L mutation blocks electron transfer not only to b_{558} but also to b_{595}, and most likely the mutation slows down the deprotonation of heme *d* and blocks the electron transfer to both *b*-type hemes. The proposed idea also contradicts the topological model where E107 is located in the middle of the membrane dielectric (*23, 27*); that makes the hypothesis unlikely.

(2) The E107 residue may be a part of a long proton channel connecting the b_{595}/d diheme site with the cytoplasm. The following observations of the present study are consistent with this proposal. (i) Formation of the oxoferryl state in the mutant is ~350-fold slower than in the wild-type enzyme. (ii) The E107L mutation decreases E_m of hemes b_{595} and *d*. (iii) Electron transfer to both *b*-type hemes from heme *d* is blocked by the mutation. (iv) Such possibility is in agreement with the predicted topology (*23, 27*).

Recently, based on the comparison of the E445A mutant and wild-type enzymes, it was suggested that there are two ionizable groups, X_P and X_N, redox-linked to the b_{595}/d diheme site (*11*). Each of the two electrons coming/leaving the diheme site should be compensated by the uptake/release of the proton by unidentified X_P and X_N groups. Meanwhile, a highly conserved E445 was proposed to be either the X_P group or the gateway in a channel that connects X_P with the periplasm (see the proposed scheme in Figure 6 of ref *11*). Unlike the E445A mutation which does not influence the extent and the rate of electron backflow, the E107L replacement severely suppresses electron redistribution from heme *d*. Location of E107 in the close proximity of heme *d* is quite unlikely because the shift of E_m of heme *d* in the redox titration is much smaller than that of other hemes. At the same time, the E107L mutation blocks deprotonation of a group located nearby heme *d* in the backflow reaction and protonation of this group during oxygen catalysis; thus it should be located in the proton-conducting channel that connects the diheme site with the cytoplasm.

Figure 6 shows a possible scheme of participation of E107 in the proton transfer pathways of cytochrome *bd*. It is clear that E107 is involved in the proton transfer to heme *d* since the E107L mutation (i) dramatically retards the oxoferryl intermediate formation in the forward oxygen reaction and (ii) virtually annuls the $\Delta\Psi$ generation in the backflow experiment. We propose that E107 is not X_N itself but rather a group in the channel delivering protons to X_N.

REFERENCES

1. Ingledew, W. J., and Poole, R. K. (1984) The respiratory chains of *Escherichia coli*. *Microbiol. Rev. 48*, 222–271.
2. Tsubaki, M., Hori, H., and Mogi, T. (2000) Probing molecular structure of dioxygen reduction site of bacterial quinol oxidases through ligand binding to the redox metal centers. *J. Inorg. Biochem. 82*, 19–25.
3. Dassa, J., Fsihi, H., Marck, C., Dion, M., Kieffer-Bontemps, M., and Boquet, P. L. (1991) A new oxygen-regulated operon in *Escherichia coli* comprises the genes for a putative third cytochrome oxidase and for pH 2.5 acid phosphatase (*app*A). *Mol. Gen. Genet. 229*, 341–352.
4. Brønstedt, L., and Atlung, T. (1996) Effect of growth conditions on expression of the acid phosphatase (*cyx-appA*) operon and the *appY* gene, which encodes a transcriptional activator of *Escherichia coli*. *J. Bacteriol. 178*, 1556–1564.
5. Sturr, M. G., Krulwich, T. A., and Hicks, D. B. (1996) Purification of a cytochrome *bd* terminal oxidase encoded by the *Escherichia coli app* locus from a Δ*cyo* Δ*cyd* strain complemented by genes from *Bacillus firmus* OF4. *J. Bacteriol. 176*, 1742–1749.
6. Cotter, P. A., Chepuri, V., Gennis, R. B., and Gunsalus, R. P. (1990) Cytochrome *o* (*cyoABCDE*) and *d* (*cydAB*) oxidase gene expression in *Escherichia coli* is regulated by oxygen, pH, and the *fnr* gene product. *J. Bacteriol. 172*, 6333–6338.
7. Rice, C. W., and Hempfling, W. P. (1978) Oxygen-limited continuous culture and respiratory energy conservation in *Escherichia coli*. *J. Bacteriol. 134*, 115–124.
8. Fu, H.-A., Iuchi, S., and Lin, E. C. C. (1991) The requirement of ArcA and Fnr for peak expression of the *cyd* operon in *Escherichia coli* under microaerobic conditions. *Mol. Gen. Genet. 226*, 209–213.
9. Puustinen, A., Finel, M., Haltia, T., Gennis, R. B., and Wikström, M. (1991) Properties of the two terminal oxidases of *Escherichia coli*. *Biochemistry 30*, 3936–3942.
10. Jasaitis, A., Borisov, V. B., Belevich, N. P., Morgan, J. E., Konstantinov, A. A., and Verkhovsky, M. I. (2000) Electrogenic reactions of cytochrome *bd*. *Biochemistry 39*, 13800–13809.
11. Belevich, I., Borisov, V. B., Zhang, J., Yang, K., Konstantinov, A. A., Gennis, R. B., and Verkhovsky, M. I. (2005) Time-resolved electrometric and optical studies on cytochrome *bd* suggest a mechanism of electron-proton coupling in the di-heme active site. *Proc. Natl. Acad. Sci. U.S.A. 102*, 3657–3662.
12. Belevich, I., Borisov, V. B., and Verkhovsky, M. I. (2007) Discovery of the true peroxy intermediate in the catalytic cycle of terminal oxidases by real-time measurement. *J. Biol. Chem. 282*, 28514–28519.
13. Mogi, T., Tsubaki, M., Hori, H., Miyoshi, H., Nakamura, H., and Anraku, Y. (1998) Two terminal quinol oxidase families in *Escherichia coli*: variations on molecular machinery for dioxygen reduction. *J. Biochem. Mol. Biol. Biophys. 2*, 79–110.
14. Poole, R. K., and Cook, G. M. (2000) Redundancy of aerobic respiratory chains in bacteria? Routes, reasons and regulation. *Adv. Microb. Physiol. 43*, 165–224.
15. Jünemann, S. (1997) Cytochrome *bd* terminal oxidase. *Biochim. Biophys. Acta 1321*, 107–127.
16. Borisov, V. B. (1996) Cytochrome *bd*: structure and properties. *Biochemistry (Moscow) 61*, 565–574. (translated from (1996) *Biokhimiya* (in Russian) *61*, 786−799).
17. Belevich, I., Borisov, V. B., Konstantinov, A. A., and Verkhovsky, M. I. (2005) Oxygenated complex of cytochrome *bd* from *Escherichia coli*: stability and photolability. *FEBS Lett. 579*, 4567–4570.
18. Miller, M. J., and Gennis, R. B. (1983) The purification and characterization of the cytochrome *d* terminal oxidase complex of the *Escherichia coli* aerobic respiratory chain. *J. Biol. Chem. 258*, 9159–9165.
19. Kita, K., Konishi, K., and Anraku, Y. (1984) Terminal oxidases of *Escherichia coli* aerobic respiratory chain. II. Purification and properties of cytochrome b_{558}-*d* complex from cells grown with limited oxygen and evidence of branched electron-carrying systems. *J. Biol. Chem. 259*, 3375–3381.
20. Meunier, B., Madgwick, S. A., Reil, E., Oettmeier, W., and Rich, P. R. (1995) New inhibitors of the quinol oxidation sites of bacterial cytochromes *bo* and *bd*. *Biochemistry 34*, 1076–1083.
21. Green, G. N., Fang, H., Lin, R.-J., Newton, G., Mather, M., Georgiou, C. D., and Gennis, R. B. (1988) The nucleotide sequence of the *cyd* locus encoding the two subunits of the cytochrome *d* terminal oxidase complex of *Escherichia coli*. *J. Biol. Chem. 263*, 13138–13143.
22. Poole, R. K. (1994) Oxygen reactions with bacterial oxidases and globins: binding, reduction and regulation. *Anthonie van Leeuwenhoek 65*, 289–310.
23. Osborne, J. P., and Gennis, R. B. (1999) Sequence analysis of cytochrome *bd* oxidase suggests a revised topology for subunits I. *Biochim. Biophys. Acta 1410*, 32–50.

24. Zhang, J., Barquera, B., and Gennis, R. B. (2004) Gene fusions with β-lactamase show that subunit I of the cytochrome *bd* quinol oxidase from *E. coli* has nine transmembrane helices with the O_2 reactive site near the periplasmic surface. *FEBS Lett. 561*, 58–62.
25. Jünemann, S., and Wrigglesworth, J. M. (1994) Antimycin inhibition of the cytochrome *bd* complex from *Azotobacter vinelandii* indicates the presence of a branched electron transfer pathway for the oxidation of ubiquinol. *FEBS Lett. 345*, 198–202.
26. Spinner, F., Cheesman, M. R., Thomson, A. J., Kaysser, T., Gennis, R. B., Peng, Q., and Peterson, J. (1995) The haem b_{558} component of the cytochrome *bd* quinol oxidase complex from *Escherichia coli* has histidine-methionine axial ligation. *Biochem. J. 308*, 641–644.
27. Mogi, T., Endou, S., Akimoto, S., Morimoto-Tadokoro, M., and Miyoshi, H. (2006) Glutamates 99 and 107 in transmembrane helix III of subunit I of cytochrome *bd* are critical for binding of the heme b_{595}-*d* binuclear center and enzyme activity. *Biochemistry 45*, 15785–15792.
28. Poole, R. K., and Williams, H. D. (1987) Proposal that the function of the membrane-bound cytochrome a_1-like haemoprotein (cytochrome *b*-595) in *Escherichia coli* is a direct electron donation to cytochrome *d*. *FEBS Lett. 217*, 49–52.
29. Kobayashi, K., Tagawa, S., and Mogi, T. (1999) Electron transfer process in cytochrome *bd*-type ubiquinol oxidase from *Escherichia coli* revealed by pulse radiolysis. *Biochemistry 38*, 5913–5917.
30. Hill, J. J., Alben, J. O., and Gennis, R. B. (1993) Spectroscopic evidence for a heme-heme binuclear center in the cytochrome *bd* ubiquinol oxidase from *Escherichia coli*. *Proc. Natl. Acad. Sci. U.S.A. 90*, 5863–5867.
31. Tsubaki, M., Hori, H., Mogi, T., and Anraku, Y. (1995) Cyanide-binding site of *bd*-type ubiquinol oxidase from *Escherichia coli*. *J. Biol. Chem. 270*, 28565–28569.
32. Borisov, V., Arutyunyan, A. M., Osborne, J. P., Gennis, R. B., and Konstantinov, A. A. (1999) Magnetic circular dichroism used to examine the interaction of *Escherichia coli* cytochrome *bd* with ligands. *Biochemistry 38*, 740–750.
33. Vos, M. H., Borisov, V. B., Liebl, U., Martin, J.-L., and Konstantinov, A. A. (2000) Femtosecond resolution of ligand-heme interactions in the high-affinity quinol oxidase *bd*: A di-heme active site? *Proc. Natl. Acad. Sci. U.S.A. 97*, 1554–1559.
34. Borisov, V. B., Sedelnikova, S. E., Poole, R. K., and Konstantinov, A. A. (2001) Interaction of cytochrome *bd* with carbon monoxide at low and room temperatures: evidence that only a small fraction of heme b_{595} reacts with CO. *J. Biol. Chem. 276*, 22095–22099.
35. Borisov, V. B., Liebl, U., Rappaport, F., Martin, J.-L., Zhang, J., Gennis, R. B., Konstantinov, A. A., and Vos, M. H. (2002) Interactions between heme *d* and heme b_{595} in quinol oxidase *bd* from *Escherichia coli*: a photoselection study using femtosecond spectroscopy. *Biochemistry 41*, 1654–1662.
36. Hori, H., Tsubaki, M., Mogi, T., and Anraku, Y. (1996) EPR study of NO complex of *bd*-type ubiquinol oxidase from *Escherichia coli*. *J. Biol. Chem. 271*, 9254–9258.
37. Arutyunyan, A. M., Borisov, V. B., Novoderezhkin, V. I., Ghaim, J., Zhang, J., Gennis, R. B., and Konstantinov, A. A. (2008) Strong excitonic interactions in the oxygen-reducing site of *bd*-type oxidase: the Fe-to-Fe distance between hemes *d* and b_{595} is 10 Å. *Biochemistry 47*, 1752–1759.
38. Borisov, V. B. (2008) Interaction of *bd*-type quinol oxidase from *Escherichia coli* and carbon monoxide: Heme *d* binds CO with high affinity. *Biochemistry (Moscow) 73*, 14–22. (translated from (2008) *Biokhimiya* (in Russian) *73*, 18−28).
39. Baughn, A. D., and Malamy, M. H. (2004) The strict anaerobe *Bacteroides fragilis* grows in and benefits from nanomolar concentrations of oxygen. *Nature 427*, 441–444.
40. Shi, L., Sohaskey, C. D., Kana, B. D., Dawes, S., North, R. J., Mizrahi, V., and Gennaro, M. L. (2005) Changes in energy metabolism of *Mycobacterium tuberculosis* in mouse lung and under in vitro conditions affecting aerobic respiration. *Proc. Natl. Acad. Sci. U.S.A. 102*, 15629–15634.
41. Loisel-Meyer, S., Jimenez de Bagues, M. P., Kohler, S., Liautard, J. P., and Jubier-Maurin, V. (2005) Differential use of the two high-oxygen-affinity terminal oxidases of *Brucella suis* for in vitro and intramacrophagic multiplication. *Infect. Immun. 73*, 7768–7771.
42. Jones, S. A., Chowdhury, F. Z., Fabich, A. J., Anderson, A., Schreiner, D. M., House, A. L., Autieri, S. M., Leatham, M. P., Lins, J. J., Jorgensen, M., Cohen, P. S., and Conway, T. (2007) Respiration of *Escherichia coli* in the mouse intestine. *Infect. Immun. 75*, 4891–4899.
43. Way, S. S., Sallustio, S., Magliozzo, R. S., and Goldberg, M. B. (1999) Impact of either elevated or decreased levels of cytochrome *bd* expression on *Shigella flexneri* virulence. *J. Bacteriol. 181*, 1229–1237.
44. Endley, S., McMurray, D., and Ficht, T. A. (2001) Interruption of the *cydB* locus in *Brucella abortus* attenuates intracellular survival and virulence in the mouse model of infection. *J. Bacteriol. 183*, 2454–2462.
45. Borisov, V. B., Forte, E., Konstantinov, A. A., Poole, R. K., Sarti, P., and Giuffre, A. (2004) Interaction of the bacterial terminal oxidase cytochrome *bd* with nitric oxide. *FEBS Lett. 576*, 201–204.
46. Borisov, V. B., Forte, E., Sarti, P., Brunori, M., Konstantinov, A. A., and Giuffre, A. (2007) Redox control of fast ligand dissociation from *Escherichia coli* cytochrome *bd*. *Biochem. Biophys. Res. Commun. 355*, 97–102.
47. Borisov, V. B., Forte, E., Sarti, P., Brunori, M., Konstantinov, A. A., and Giuffre, A. (2006) Nitric oxide reacts with the ferryl-oxo catalytic intermediate of the Cu_B-lacking cytochrome *bd* terminal oxidase. *FEBS Lett. 580*, 4823–4826.
48. Otto, H., Marti, T., Holz, M., Mogi, T., Lindau, M., Khorana, H. G., and Heyn, M. P. (1989) Aspartic acid-96 is the internal proton donor in the reprotonation of the Schiff base of bacteriorhodopsin. *Proc. Natl. Acad. Sci. U.S.A. 86*, 9228–9232.
49. Mogi, T., Stern, L. H., Marti, T., Chao, B. H., and Khorana, H. G. (1988) Aspartic acid substitutions affect proton translocation by bacteriorhodopsin. *Proc. Natl. Acad. Sci. U.S.A. 85*, 4148–4152.
50. Yang, K., Zhang, J., Vakkasoglu, A. S., Hielscher, R., Osborne, J. P., Hemp, J., Miyoshi, H., Hellwig, P., and Gennis, R. B. (2007) Glutamate 107 in subunit I of the cytochrome *bd* quinol oxidase from *Escherichia coli* is protonated and near the heme *d*/heme b_{595} binuclear center. *Biochemistry 46*, 3270–3278.
51. Berry, E. A., and Trumpower, B. L. (1987) Simultaneous determination of hemes *a*, *b*, and *c* from pyridine hemochrome spectra. *Anal. Biochem. 161*, 1–15.
52. Belevich, I., Bloch, D. A., Belevich, N., Wikstrom, M., and Verkhovsky, M. I. (2007) Exploring the proton pump mechanism of cytochrome *c* oxidase in real time. *Proc. Natl. Acad. Sci. U.S.A. 104*, 2685–2690.
53. Belevich, I., Borisov, V. B., Bloch, D. A., Konstantinov, A. A., and Verkhovsky, M. I. (2007) Cytochrome *bd* from *Azotobacter vinelandii*: evidence for high-affinity oxygen binding. *Biochemistry 46*, 11177–11184.
54. Koland, J. G., Miller, M. J., and Gennis, R. B. (1984) Potentiometric analysis of the purified cytochrome *d* terminal oxidase complex from *Escherichia coli*. *Biochemistry 23*, 1051–1056.
55. Jünemann, S., Wrigglesworth, J. M., and Rich, P. R. (1997) Effects of *dec*yl-aurachin D and reversed electron transfer in cytochrome *bd*. *Biochemistry 36*, 9323–9331.
56. Lorence, R. M., Koland, J. G., and Gennis, R. B. (1986) Coulometric and spectroscopic analysis of the purified cytochrome *d* complex of *Escherichia coli*: evidence for the identification of "cytochrome a_1" as cytochrome b_{595}. *Biochemistry 25*, 2314–2321.
57. Lorence, R. M., Carter, K., Gennis, R. B., Matsushita, K., and Kaback, H. R. (1988) Trypsin proteolysis of the cytochrome *d* complex of *Escherichia coli* selectively inhibits ubiquinol oxidase activity while not affecting *N*,*N*,*N*′,*N*′′- tetramethyl-*p*-phenylenediamine oxidase activity. *J. Biol. Chem. 11*, 5271–5276.

BI800435A